SAND2008-1676C

Fiber faceplates to mitigate diffraction effects in an imaging snapshot polarimeter

A. A. Cruz-Cabrera[1], S. A. Kemme[1] and T. R. Carter[2]

ABSTRACT

We investigate the advantages of employing a fiber faceplate in a snapshot polarimetry system. Our previous work at Sandia National Laboratories indicates that diffraction and propagation between the micropolarizer array, the micro-waveplate array, and the Focal Plane Array (FPA) degrade performance, as quantified by the extinction ratio[1,2]. Crosstalk between adjacent pixels due to diffraction increases uncertainty of the measured polarization states in a scene of interest. These issues are exacerbated in the long-wavelength regime and as FPA pixel dimensions decrease.

One solution, since it minimizes propagation distance, is to construct the micropolarizer and micro-waveplate arrays on a single substrate surface and to place this combination on the FPA[3]. This solution is a significant fabrication challenge and decreases yield due to its serial assembly nature.

An alternative solution that would improve yield is to fabricate the micropolarizer on top of a fiber faceplate, place the faceplate on the FPA with the micropolarizer facing away, then place the waveplate array on top of the micropolarizer. The optical field that passes through the plane of the microwaveplate array and the micropolarizer array is guided to the FPA plane, without suffering diffraction effects associated with free-space propagation. We will quantify the utility of these proposed configurations with predicted imaging polarimetric system extinction ratios.

Keywords: polarimetry, faceplates, snap-shot, imaging, LWIR, MWIR, fiber, focal plane array

1. INTRODUCTION

There is a significant level of interest in capturing polarization information from an imaged scene in both the mid-wave infrared (MWIR) and long-wave infrared (LWIR). Of the several techniques available[4-7], snapshot[8-10] polarimetry is of great interest given the significance of capturing the four Stokes parameters from dynamic scenes. The usual method of implementing snapshot polarimetry is to fabricate the three components separately, each on their own substrates: the microwaveplate array usually in a high refractive index material; the micropolarizer on a low refractive index substrate; and the FPA on a semiconductor substrate. The three components are then assembled by gluing the micro-polarizer on top of the FPA, and the microwaveplate on top of the micropolarizer, see figure 1(a).

Previous work[1,2] has indicated that for typical micropolarizer sizes, dimensions on the order of 2 to 12 waves, will diffract light in such a way that crosstalk between adjacent pixels is enough to generate uncertainty about the polarization state of the field being imaged. This situation worsens as the pixel sizes decrease with respect to the wavelength and the distance increases between the pixelated micropolarizer/microwaveplate array and the FPA. Figure 1(b) shows two experimentally measured images[1-3] from a micropolarizer array at two distances in free space, 0 and 152 micrometer for an input wavelength of 3.39 μm. The 152μm thickness is optically equivalent to a glass substrate of 225μm. The importance of the second image is the increased crosstalk between adjacent pixels and the loss of the original pixel intensity profiles. This leads to increased error in the measurement of the polarization state of the imaged field.

[1]Sandia National Laboratories, Albuquerque, NM 87185-1082
[2]L&M Technologies, Albuquerque, NM 87123

In section two, we will introduce a practical approach to reduce diffraction, therefore crosstalk, by guiding the image of the microwaveplate and micropolarizer array using a fiber optics faceplate. The next section will compare simulated results with experimental data from previous work to ascertain the validity of our model. The third section will quantify performance with modeling results of a faceplate imaging a checkered light source, intended to simulate the transmission from a micropolarizer array.

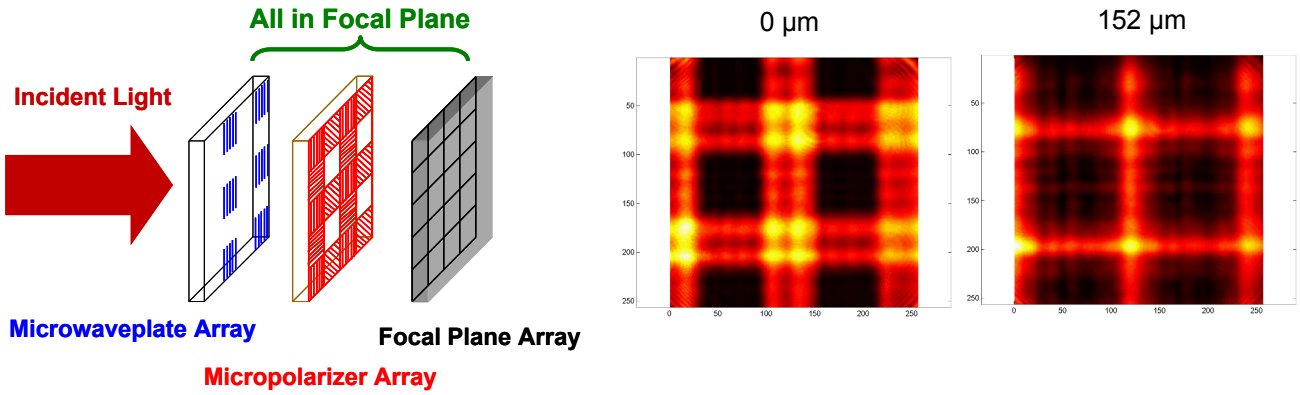

Figure 1 Panel (a) depicts the traditional way of assembling an imager that implements four-state snapshot polarimetry. The different components are fabricated on their own substrates: microwaveplate, micropolarizer and the FPA. Unfortunately, diffracted light will have to propagate across a significant distance through a substrate. Diffraction increases crosstalk between adjacent pixels. Panel (b) depicts an experimentally measured infrared image (at a wavelength of 3.39μm) of a micropolarizer array, 0μm, and 152μm in free space (respectively) from the polarizer plane. Notice the increase in diffracted light in the black areas where there should not be any light.

2. APPROACH

The key to this approach is to replace the substrate used to fabricate the micropolarizer array with a fiber optic faceplate. For the applications in the MWIR, the faceplates could be made with heavy metal fluoride glass (HMFG) fibers[11]. These materials typically have a low refractive index, around 1.45. A low index is important for a desired extinction ratio and transmission of TM light, a low refractive index glass requires smaller aspect ratio for the wiregrid polarizers[12]. Other fibers have larger indices: chalcogenide is on the order of 2.6 to 2.9, germanate fibers are about 1.8, and crystal fibers are 2.2[11]. Since the HMFG fibers cannot be used at the LWIR range due to increased loss at wavelengths larger than 5 microns, some of the crystal and chalcogenide fibers could be considered as alternatives.

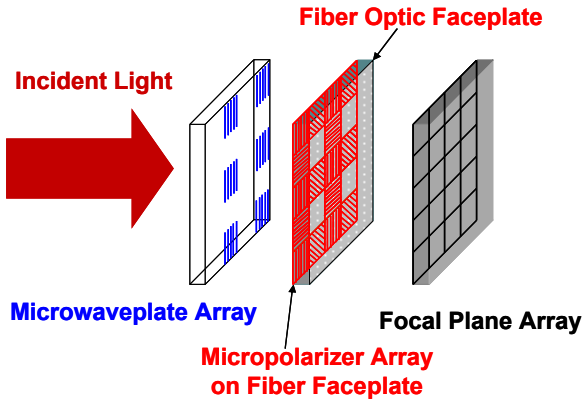

Figure 2 The solution we propose is to fabricate the micropolarizer array on top a fiber optic faceplate. The microwaveplate array can be aligned and glue on top of the micropolarizer array, the microwaveplate array and the micropolarizers are facing each other. The fiber optic faceplate will guide the image of the two arrayed devices to the FPA.

After fabricating the micropolarizer array on the faceplate, then it can be integrated with the FPA. The micropolarizer array will be facing the microwaveplate and away from the FPA, figure 2. Placing the micropolarizer array facing the FPA and away from the microwaveplate does not work because the fiber faceplate scrambles the polarization of the incident light. Intensity and contrast ratio are the only important parameters after the micropolarizer and they are well preserved by the faceplate.

2. VERIFYING MODELING TOOL

To verify our model we began with data from a previous set of experiments where a 4 x 4 μm VCSEL illuminated a fiber array[13] at a wavelength of 0.85 μm. The experiments employed Schott[14] fiber image guides (FIG) with numerical apertures (NA) of 0.257, 0.537, and 1.00. We used the measurements of the FIG with NA of 0.537 to verify the behavior of our model. The FIG has a 200mm length, a hexagonal cross section with 9.1μm core diameter, with cladding diameter of 13.1μm, and a pitch of 13.5μm. The core and cladding refractive indices are 1.58 and 1.486 respectively. In the measurement, a 4 x 4 μm VCSEL is placed at ~0μm and at 100μm from the FIG input face. The fibers at the extreme ends are physically bundled by an acid soluble glass (ASG) which fixes their relative positions. The ASG has been removed through most of the length of the FIG.

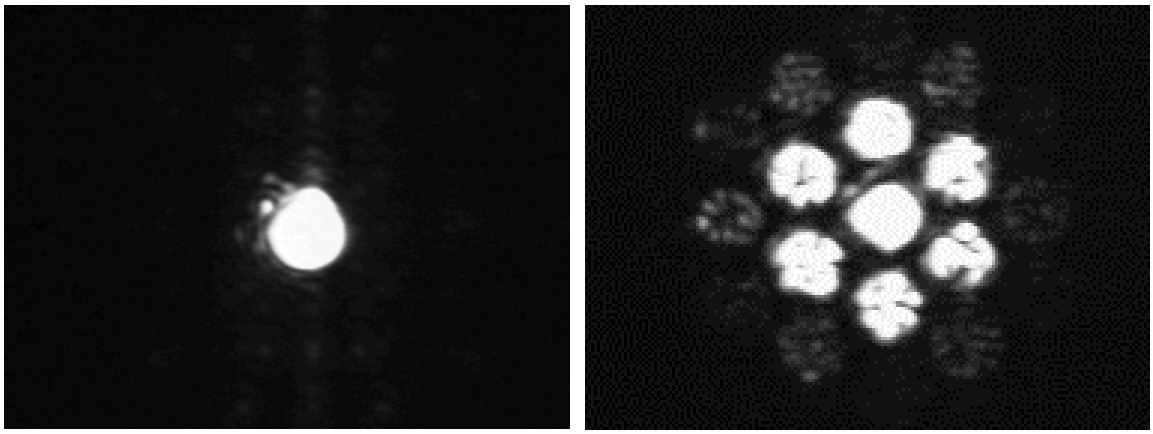

(a) **(b)**

Figure 3 Image from measurement indicating that we get an average of 65.6% transmitted through the fiber array, shown in panel (a), when the VCSEL is placed 0 to 1μm away from the fiber array. Panel (b) shows a 38.6% transmission when the VCSEL is located 100μm away from the input of the fiber array.

A non-sequential ray tracing software was used to model the system. It uses a square source with the same dimensions of the VCSEL. The divergence of the VCSEL is defined in the model by the relation:

$$I(\theta) \approx I_0(\cos(\theta))^{C_n} \quad where\ C_n > 0 \tag{1}$$

C_n was estimated to be ~25, for an NA of 0.38. In our simulation, the VCSEL is located at 1μm and 100μm from the FIG input face. The model has 14 x 14 fibers arrayed in a hexagonal pattern. The pitch between fibers is the same 13.5μm. Each core is defined as a cylindrical volume and each cladding as an annular volume concentrically aligned to the core. Both volumes have the same refractive indices and dimensions as the experiment. The model did not have ASG through the length of the fibers, instead the interfiber gaps are air.

The first experiment sets the VCSEL at ~0μm from the FIG and center on one fiber. An L-I curve reports an efficiency at the output of the FIG between 72.7% and 54.8%, with an average of 65.6%, see figure 3(a), for a current range of 1 to 7 milliamps. This first measurement is simulated in our model and reports 63.7%, figure 4(a). The second experiment places the VCSEL at 100μm from the FIG and again laterally center on one fiber. The L-I curve measurement gives efficiencies at the output of the FIG between 39.8% and 34.4%, with an average of 38.6%, see figure 3(b). The same setup is realized in our model and predicts efficiencies of 29.4%, figure 4(b). The difference in magnitude between the

experiment and the non-sequential model can be attributed to the materials utilized between the fibers. The FIG in the experiment has an acid soluble glass as the gap filler at the extreme ends, which has a high refractive index of 1.61, On the other hand, the non-sequential model does not have the ASG, but air with a unity index of refraction. The following section shows the role gap fillers have in the performance of the faceplate. These results give us confidence that we can use the modeling tool to verify the faceplate performance and its suitability implementing four Stokes snapshot polarimetry.

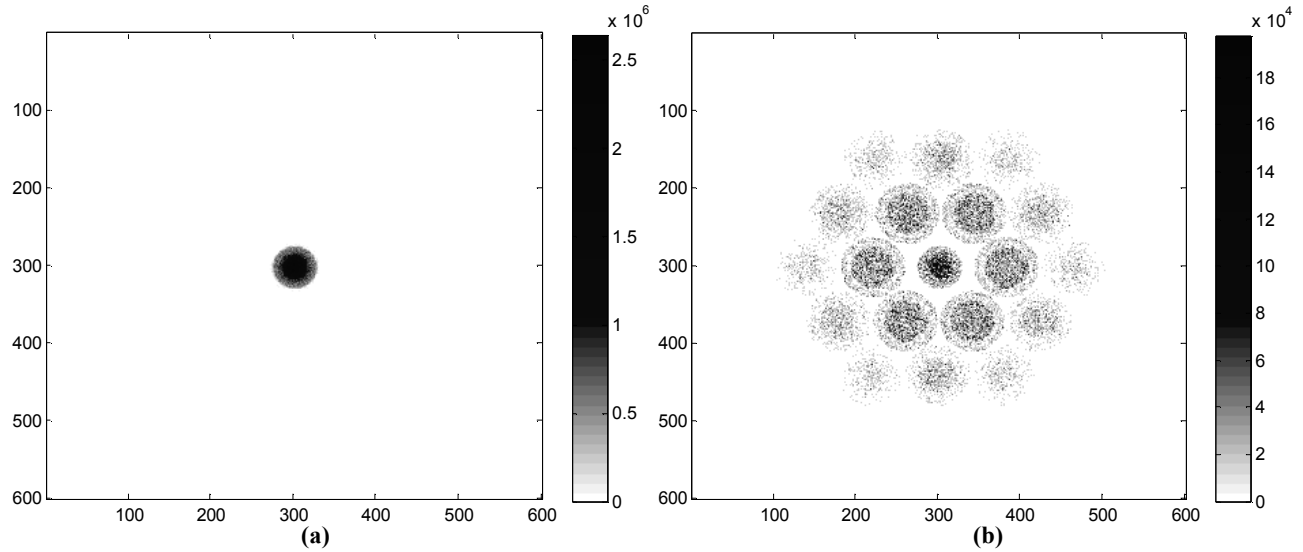

Figure 4 Graphs from non sequential ray tracing indicating that we get 63.7% transmitted through the fiber array, shown in panel (a), when the VCSEL is placed 1μm away from the fiber array. Panel (b) shows a 29.4% transmission when the VCSEL is located 100μm away from the fiber array.

3. NON-SEQUENTIAL MODEL OF FACEPLATE

To implement the faceplate using the non-sequential model we use refractive indices for the core and the cladding similar to the ones used in the experiment with the FIG. Possible variations in cladding and core refractive index allow access to a full range of faceplate NAs from 0.1 to 1. These refractive indices would be consistent for a waveplate based on HMFG or germanate materials.

The model starts with a checkered, amplitude source pattern to simulate the field transmitted by the pixelated micropolarizer, figure 5(a). Each pixel source has its own divergence to represent the diffraction effects of a range of wavelengths for a specific pixel aperture size. Equation 1 defines this divergence in the model. We describe a source pixel NA for angles where the intensity is at the $1/e^2$ of the I_0 value. We used C_n= 5.5 for NA= 0.7; C_n= 133 for NA= 0.17; and C_n= 535 for NA= 0.09. The pixels are 30μm wide. Four of the pixels have a unity power, representing an incident electric field perpendicular to the wiregrids of an ideal polarizer. Other four pixels will have half unity power, representing a 45° and/or 135° orientation of wiregrids with respect to the incident electric field for naturally polarized incident light. Eight pixels have zero light, representing an ideal polarizer with the wiregrids oriented at 0 degrees from the electric field.

The main parameter that we calculate in the model is extinction ratio after the faceplate. This allows us to compare the effects of a faceplate with an ordinary substrate. The model has a faceplate that is 0.5-millimeter thick, with a fiber pitch of 10μm and set in a rectangular array. The rectangular array is necessary to properly integrate with the FPA pixels. The fibers have 8μm diameter cores with a 10μm diameter cladding. We varied the core and cladding refractive indices to obtain several NAs that vary from 0.1 to 1. The NA of the fiber can be calculated from:

$$NA = \left(n_{core}^2 - n_{cladding}^2\right)^{1/2} \tag{2}$$

Figure 5(b) shows the light after propagating through the faceplate. Comparison of figure 5(a) with 5(b) shows that the intensity profile from the microwaveplate-micropolarizer plane is successfully guided to the FPA plane. The extinction ratio between one of the unity power pixels (dotted black square) and a zero light pixel (dashed black square) is 24:1. Removing the faceplate from the system shows that the image is completely lost to diffraction, see figure 5(c), and it measures an extinction ratio of 1.3:1. In this case, the pixel source NA is 0.7 and the faceplate NA is 0.537; the core and cladding refractive indices are 1.58 and 1.486, respectively. The gap between the fibers is air for this case.

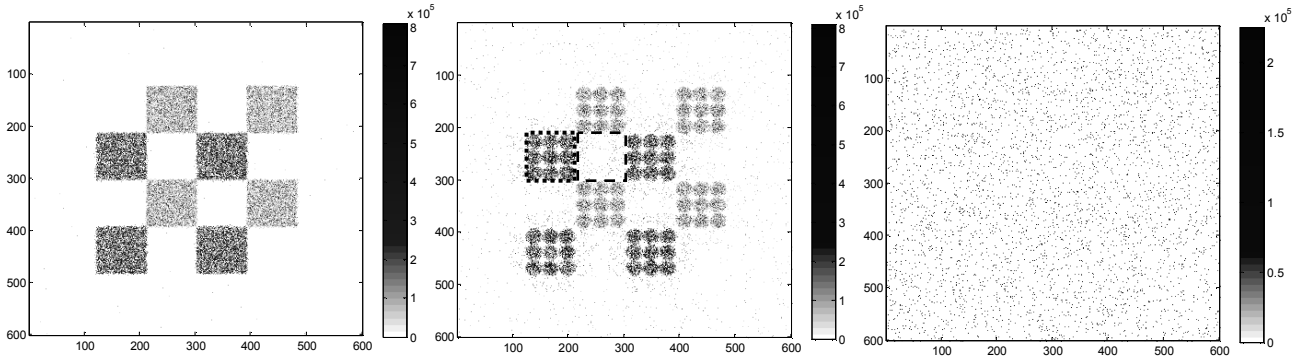

(a) **(b)** **(c)**

Figure 5 Panel (a) shows the square sources with a source NA of 0.7 in the non-sequential model. The sources are two microns away from the faceplate and the detector is one micron. The eight square sources are arranged in a checkerboard fashion, four of them have a unit of power, and the other four have half the power. Panel (b) shows the image at the other side of the faceplate, with an extinction ratio between the unit power pixel (dotted black square) and the blank pixel (dashed black square) of 24:1 for a faceplate with fiber NA of 0.537. Panel (c) shows the irradiance distribution at the same plane as in Panel (b) but without a faceplate and measures an extinction ratio of 1.3:1.

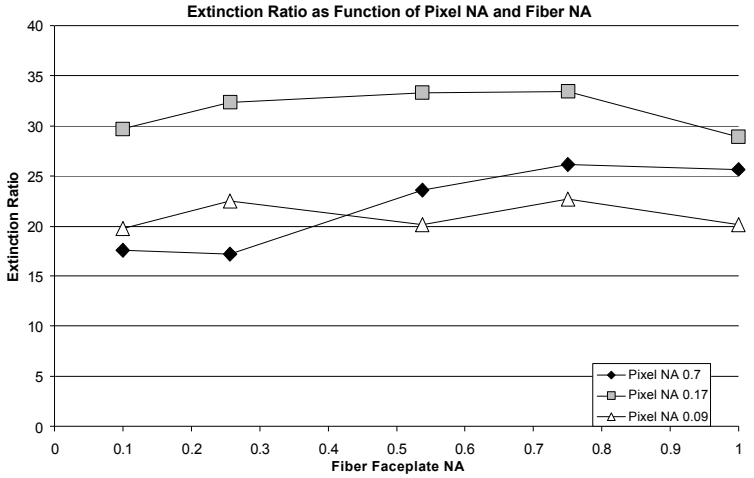

Figure 6 Extinction ratio curves for different faceplate fibers NA and three types of source pixel NA. The source pixel NA is a way to represent the diffraction at the aperture of the pixels. The non-sequential tool emits the rays using a cosine distribution and we selected a $1/e^2$ cut-off to define the NA of the pixel. The curves indicate that low source pixel NAs (little diffraction) do not necessarily mean higher extinction ratio

We examined the effect of the faceplate-fiber NA and the source pixel NA on the extinction ratio value, figure 6, and is remarkable that the overall highest extinction ratio is for the pixels with NA= 0.17 and not the pixels with the smallest pixel NA= 0.09. Additionally, as the pixel NA decreases, the need for a faceplate decreases too since this corresponds to decreasing amounts of diffraction. For the case where the pixel NA is 0.09, figure 7, the extinction ratio is 20:1 with a faceplate and 4:1 without it. As the source NA gets even smaller, the extinction ratio without a faceplate increases. This will be valid when the pixel size is larger than the wavelength by a factor greater than 30, leading to reduced diffraction.

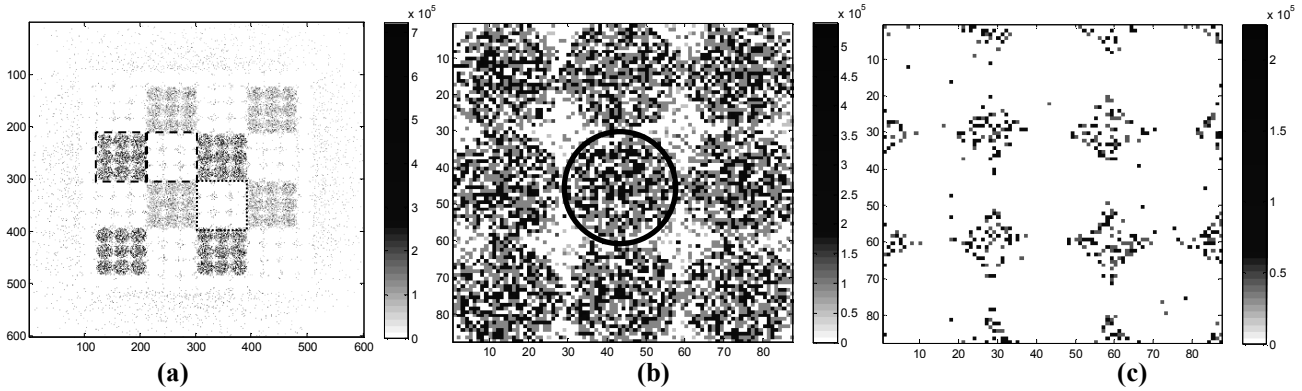

Figure 7 Panel (a) shows the two pixels used in the calculation of extinction ratio (dashed black lines). The dark pixel is surrounded by four pixels that are transmitting light, only the diagonal, lower-right pixel has the same characteristic (dotted black line). Panel (b) shows high intensity pixel, where the fibers are obvious, (black circle). Panel (c) shows light bleeding from adjacent pixels that couples in the spaces between fibers. The fiber faceplate NA is 0.53, the source pixel NA is 0.09, and the resulting extinction ratio is 20:1.

The simulation with the low-light pixel, figure 7(c), indicates that the extinction ratio is sensitive to the refractive index of the interfiber gap filler. The extreme ends of the FIG in Mukherjee's[13] experiment had the fibers filled with an ASG, with n= 1.61. To examine the effect of the gap refractive index, we modeled the faceplate with fiber gap filler indices of 1, 1.2, 1.486, 1.61, and 2. Figure 8 shows that the optimum extinction ratio occurs when the fiber gap filler has a refractive index of 1. We again used the fiber core refractive index of 1.58 and the cladding index of 1.486 for a fiber NA of 0.537. It was expected that the extinction ratio would grow by increasing the gap filler refractive index to larger values than the index of the cladding, but the increase only provided a small raise in extinction ratio.

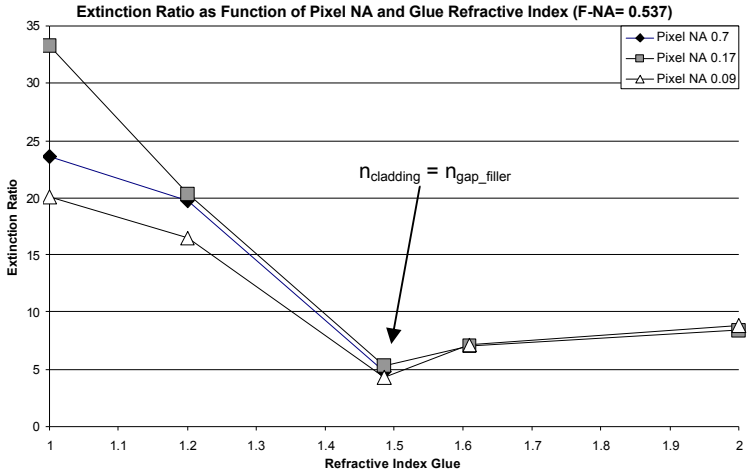

Figure 8 Extinction ratio curves for different refractive indices for the interfiber gap fillers. The optimum configuration is obtained for a refractive index of 1. As the index increases, the extinction ratio decreases to a value close to five when the refractive index matches the cladding. The fiber NA for this faceplate is 0.537, with a core of 1.58 and a cladding of 1.486.

We noticed a subtlety with this analysis approach. We used a faceplate with a fiber NA of 0.537, the core refractive index is 1.58, and the cladding is 1.486. However, from Equation 2 above, it is possible to obtain the same NA with a different pair of refractive indices, e.g. n_{core}= 1.8, $n_{cladding}$= 1.718. The resulting extinction ratio of the faceplate will change, see figure 9. Of course, changing the core and cladding may not be an option for the faceplate; however, the gap filler may be an easier parameter to modify.

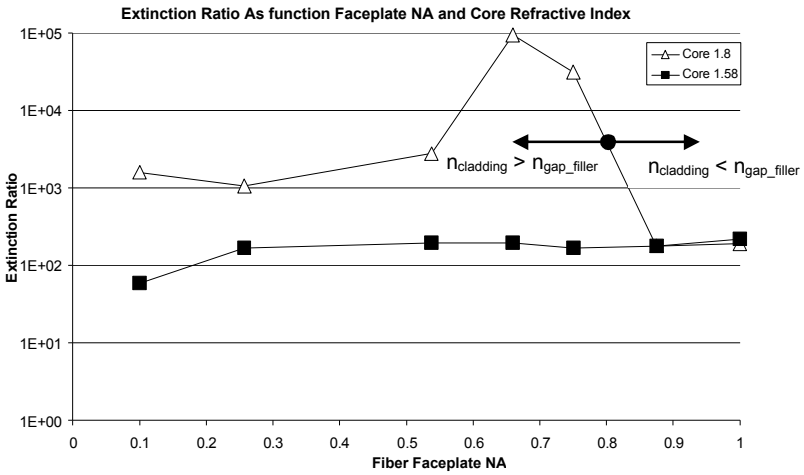

Figure 9 Extinction ratios as function of fiber faceplate NA for two core refractive indices: 1.58 and 1.8. The gap filler is absorptive and has a refractive index n= 1.61+i0.00171. The absorptive gap filler increases the extinction ratio by a factor of five for the core with n= 1.58. For a core with n=1.8 the increase factor is 30 to 1000 when the cladding refractive index is larger than the refractive index of the gap filler; when the cladding is lower the increase in extinction ratio is by a factor of five.

Having an absorptive gap filler should eliminate the light propagation between the fibers and increase the extinction ratio. For a fully absorptive gap filler, and no other sources of TE crosstalk, the degradation of the extinction ratio through the faceplate is eliminated and the simulated output has an infinite extinction ratio. A more realistic absorptive gap filler could have a refractive index n= 1.61 and transmit 1% through a one millimeter substrate, or an equivalent n= 1.61+i0.00171. Figure 9 shows the extinction ratio performance with a gap filler of this refractive index. The figure shows the extinction ratios as function of fiber faceplate NA for two core refractive indices: 1.58 and 1.8. The absorptive gap filler increases the extinction ratio by a factor of five for the core with n= 1.58. The cladding refractive index does not exceed the refractive index of the gap filler for any case. For a core with n=1.8 the increase factor is 30 to 1000 when the cladding refractive index is larger than the refractive index of the gap filler. When the cladding is lower, the increase in extinction ratio is a factor of five.

5. CONCLUSIONS

We have shown a method to fabricate in a realistic way a snapshot polarimeter that can characterize the four Stokes' parameters. Implementing snapshot polarimetry with individual substrates for each element results in low extinction ratios. Diffraction effects due to the aperture of the pixels increase crosstalk and reduce extinction ratio. We propose to exchange the micropolarizer substrate with a fiber optic faceplate. The faceplate should be made of materials used in fibers that work in the infrared, such as heavy metal fluoride glass (HMFG) for the MWIR or chalcogenide for the LWIR range. Our analyses include various divergences of the light incident upon the faceplate and various fiber NAs within the faceplate. The extinction ratio was optimum for the configuration with a fiber NA near 0.5 and a light source divergence of 10 degrees. For faceplates without gap fillers, the extinction ratio is between 17:1 and 33:1 for all faceplate fiber NAs and source light divergences. We considered different refractive indices for the gap filler and noticed that the extinction ratio diminishes to 5:1 when the refractive index is the same for the interfiber gap filler and the cladding, and barely increasing at larger refractive indices. If the refractive index is complex, the material is absorptive, and the extinction ratio increases to 170:1 when $n_{cladding} < n_{gap\_filler}$ and increases to 30000:1 when $n_{cladding} > n_{gap\_filler}$.

Further work should be done to realize this approach. We want to quantify the lateral position tolerance of the faceplate with respect to the micropolarizer array. Clearly, a misalignment will lead to crosstalk into adjacent pixels. We should look at performance variations between fiber array geometries such as rectangular and hexagonal. Moreover, we can characterize modeled predictions of extinction ratio with fiber dimensions. Finally, we need to fabricate these configurations and confirm our modeling predictions with measurement.

ACKNOWLEDGMENT

Sandia is a multiprogram laboratory operated by Sandia Corporation, a Lockheed Martin Company, for the United States Department of Energy's National Nuclear Security Administration under contract DE-AC04-94AL85000.

REFERENCES

1. S.A. Kemme, A.A. Cruz-Cabrera, P. Nandy, R.R. Boye, J.R. Wendt, T.R. Carter, and S. Samora "Micropolarizer Arrays in the MWIR for Snapshot Polarimetric Imaging," Proc. of the SPIE – The International Society for Optical Engineering, Orlando, FL, **6556**, May 2007.

2. A. A. Cruz-Cabrera, S.A. Kemme, J.R. Wendt, R.R. Boye, T.R. Carter, and S. Samora, "Polarimetric Imaging Cross Talk Effects from Glue Separation Between FPA and Micropolarizer Arrays in the MWIR," Proc. of the SPIE – The International Society for Optical Engineering, San Jose, CA, **6478**, Feb 2007.

3. S.A. Kemme, A.A. Cruz-Cabrera, R.R. Boye, T.R. Carter, and S. Samora, C. Alford, J.R. Wendt, G.A. Vawter, J.L. Smith, "Micropolarizing Device for Long Wavelength Infrared Polarization Imaging," **SAND2006-6889**, Sandia National Laboratories, Nov 2006.

4. O. Matoba and B. Javidi, "Three-dimensional polarimetric integral imaging," Opt. Lett., **29**, 2375-2377, 2004.

5. J. Peterson, G. L. Jensen, J. A. Kristi, and J. A. Shaw, "Polarimetric imaging using continuously spinning polarizer element," Proc. SPIE, **4133**, 292-300, 2000.

6. D. S. Sabatke, A. M. Locke, M. R. Descour, W. C. Sweatt, J. P. Garcia, E. L. Dereniak, S. A. Kemme, and G. S. Phipps, "Figures of merit for complete Stokes polarimeter optimization," Proc. SPIE, **4133**, 75-81, 2000.

7. D. S. Sabatke, M. R. Descour, E. L. Dereniak, W. C. Sweatt, S. A. Kemme, and G. S. Phipps, "Optimization of retardance for complete Stokes polarimeter," Opt. Lett., **25**, 802-804, 2000.

8. G. P. Nordin, J. T. Meier, P. C. Deguzman, and M. W. Jones, "Micropolarizer array for infrared imaging polarimetry," J. Opt. Soc. Am. A., **16**, 1168-1174, 1999.

9. J. Guo and D. J. Brady, "Fabrication of high-resolution micropolarizer arrays," Opt. Eng., **36**, 2268-2271, 1997.

10. J. Guo and D. J. Brady, "Fabrication of thin-film micropolarizer arrays for visible imaging polarimetry," App. Opt., **39**, 1486-1492, 2000.

11. J. A. Harrington, "Infrared Fiber Optics," at http://irfibers.rutgers.edu/pdf_files/ir_fiber_review.pdf, 2000.

12. A. A. Cruz-Cabrera, S. A. Kemme, J. R. Wendt, R. R. Boye, T. Carter, and S. Samora, "Fabrication and testing of finite aperture polarizers for determination of edge termination effects on polarimetric imaging applications at midwave infrared," J. Micro/Nanolith. MEMS MOEMS, **7**, Jan-Mar, 2008.

13. S. D. Mukherjee, K. D. Choquette, K. M. Geib, G. R. Hadley, T. R. Carter, A. J. Fischer, C. T. Sullivan, and K. Tatah, " Characterization of Crosstalk Sources in Massively Parallel Datalinks Using VCSEL Arrays and Fiber Image Guides," Opt. in Comp., OThA6, Lake Tahoe, NV, 2001.

14. S. D. Mukherjee, K. M. Geib, K. D. Choquette, and M. Robinson, "Input Coupling Measurements for Parallel Optical Interconnects using Imaging Fiber Bundles and VCSEL Arrays," Conference Digest 2000 CLEO-Europe, CWJ2, 267, Nice, France, 2000.